Waveform timing performance of a 5 GS/s fast pulse sampling module with DRS4 [*]

WANG Jin-Hong(王进红)[1,2]   LIU Shu-Bin(刘树彬)[1,2]   AN Qi(安琪)[1,2]

[1] State Key Laboratory of Particle Detection and Electronics, University of Science and Technology of China, Hefei 230026 China
[2] Department of Modern Physics, University of Science and Technology of China, Hefei 230026, China

Abstract: We first clarify timing issues of non-uniform sampling intervals regarding a 5 GS/s fast pulse sampling module with DRS4. A calibration strategy is proposed, and as a result, the waveform timing performance is improved to below 10 ps RMS. We then further evaluate waveform-timing performance of the module by comparing with a 10 GS/s oscilloscope in a setup with plastic scintillators and fast PMTs. Different waveform timing algorithms are employed for analysis, and the module shows comparable timing performance with that of the oscilloscope.

1   Introduction

There are several TOF systems in high energy experiments utilizing long plastic scintillator bars [1–3]. In these systems, the two ends of each bar are read out via PMTs, and corresponding pulses from the PMTs are transmitted to front-end signal processing circuits as leading-edge discriminators for the arrival time of particles. With the progress of modern technology, it is now conceivable to read out the scintillators with fast PMTs for better timing performance, with upgrade of the associated readout electronics also needed. It is pointed out in Refs. [4, 5] that waveform sampling gives the best timing precision compared with conventional timing techniques such as leading edge discriminators, constant fraction discriminators and multiple threshold discriminators. Traditionally, one uses analogue-to-digital converters (ADCs) for pulse sampling in physics experiments [6–12]. Recent studies show that waveform sampling with switched-capacitor arrays (SCAs) is also a promising technique in consideration of system densities, power consumption and financial cost [13–19]. Up to now, several Application Specific Integrated Circuits (ASICs) of SCAs for high-energy physics experiments have been developed [18–22]. A review of the representative SCAs can be found in Ref. [23].

In our previous work [23], we chose DRS4 [22, 24], the fourth version of the Domino Ring Sampler (DRS) from the Paul Scherrer Institute (PSI), Switzerland, and built a 5 GS/s fast sampling module. The module is proved to be capable of sub-10 ps RMS waveform timing after a series of calibration strategies [23–25]. In this work, we first continue our effort to clarify issues regarding non-uniform sampling intervals of the module. Then we evaluate its timing performance in a cosmic ray setup with plastic scintillators and fast PMTs. The timing performance is also compared with that of a Lecroy 10 GS/s oscilloscope [26] in a similar setup for evaluation of possibilities to improve timing performance of TOF systems [27].

We arrange this paper as follows. In Section 2, we clarify issues regarding uneven sampling intervals of the module. In Section 3, we evaluate the timing performance of the module by putting it in a cosmic ray telescope with plastic scintillator bars and PMTs, and compare the timing performance with that of the 10 GS/s oscilloscope. Discussion is given in Section 4. Finally, in Section 5, we conclude this paper and summarize what we have achieved.

2   Timing issues regarding the module

There are several factors limiting the potential timing performance of the module, such as the analog input bandwidth and maximum sampling rate of the module, as well as the performance optimization of DRS4. Generally, a higher bandwidth and sampling rate results in better timing performance [4, 5]. The analog bandwidth of DRS4 can be as high as 950 MHz [24]. However, this will drop dramatically without a proper arrangement of

the input driving circuits for the heavy capacitive load at its input. The achieved bandwidth of the module in Ref. [23] is around 600 MHz with fully differential amplifiers. We operate the module at around the highest sampling rate of the DRS4, 4.7 GS/s per channel. Figure 1 is a photograph of the module; a detailed description is given in Ref. [23].
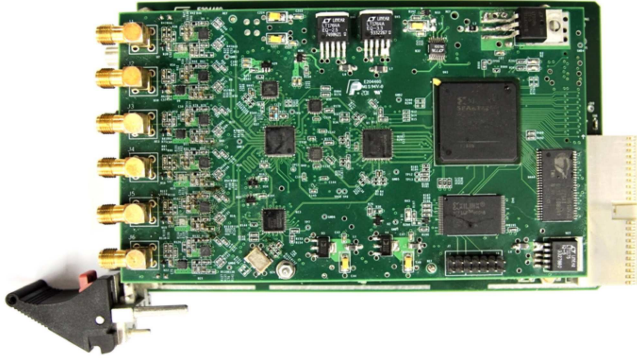

Fig. 1.   (color online) A photograph of the fast sampling module.

Once the module is fabricated, its analog bandwidth and maximum sampling rate are relatively fixed. We improve its timing precision by optimizing the performance of the DRS4, as DC offset compensation, and uneven sampling intervals calibration. The DC offset is the variation of residual voltage in each sampling cell of DRS4, and this variation after compensation can be as low as 0.35 mV RMS [23]. The uneven sampling intervals of DRS4 are a bit more complex to calibrate. In Ref. [23], we proposed to do this with zero crossing of sine waves. In the signal processing, the sinusoidal samples are pre-processed with a low-pass filter before applying the zero-crossing algorithm. The sampling intervals obtained show very small variation ($\sim$5 ps RMS at 4.7 GS/s), and good performance of the module is achieved after uneven sampling interval calibration and noise suppression. However, we find that the distribution of the sampling intervals obtained in Ref. [23] cannot reflect the real delay variation of the domino taps in DRS4, in spite of the good performance achieved. We clarify this as follows.

2.1   Variation of sampling intervals of DRS4

We determine the sampling intervals of DRS4 with zero-crossing of sine waves [23]. The sine frequency is 100 MHz, and it is sampled at 4.7 GS/s. In Ref. [23], a low-pass filter was applied to the sinusoidal samples before performing the zero-crossing algorithm; here, the filter is removed and raw sinusoidal samples are used for analysis. We plot several trials of sine waveforms with respect to the sampling cell number in Fig. 2. The samples of each trial are arranged in an ascending sequence

of the 1024 sampling cells in DRS4 (from cell 1 to 1024). For clarity, we show only part of the waveforms (from cell 800 to cell 850). The analog outputs from DRS4 are digitized with a 14-bit ADC in the module [23]. Theoretically, the sampled sine waves should be smooth everywhere with uniform sampling. However, we observe that there is an up-down alternation of the samples in Fig. 2. Moreover, this upward or downward trend at a sampling cell is constant for samples within the same rising or falling edges, e.g., samples at cell 810 show an upward trend in the falling edges, whereas those at cell 830 exhibit a downward tendency in the rising edges.
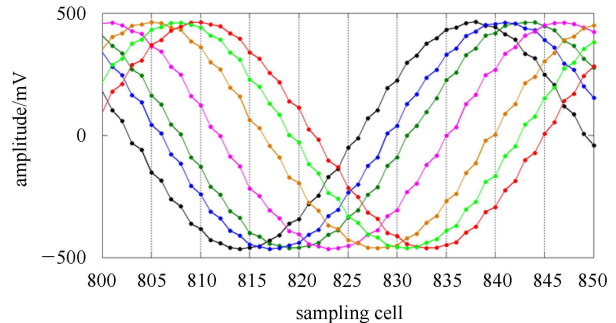

Fig. 2.   (color online) Up-down alternation of sampled sine points.

For a given sine, $V(t) = V_0 \times \sin(\omega t + \varphi)$, where ω is the angular frequency and φ is its phase. The voltage difference (ΔV) between two adjacent sampled points across zero is constant in an ideal case (uniform sampling and no voltage distortion): $\Delta V = \omega \times V_0 \times \Delta t$, where Δt is the sampling interval. We collect the zero-crossing voltage difference of each sampling cell, and plot the results in Fig. 3. Figure 3(a) shows ΔV at each sampling cell. The voltage difference per cell is given by an average of hundreds of trials. Figure 3(b) presents the corresponding distribution of ΔV for the total 1024 sampling cells. We observe that the voltage difference alternates cell by cell, and is spread into two distributions: one is centralized at about 81 mV, and the other at about 40 mV. The variations of the two distributions are both around 6.7 mV RMS. Figure 3(c) shows the standard deviation of ΔV at each sampling cell. The variation of ΔV at each cell is around 1 mV RMS, which shows that the corresponding zero-crossing voltage difference is quite stable. We can therefore derive the sampling intervals from these voltages.

At the sine zero-crossing point, the voltage difference is proportional to the sampling intervals. Therefore from the voltage differences in Fig. 3(a), we can derive the ratio of the 1024 tap delay in DRS4. Taking into account that the total sampling interval equals $1024 \times 1/f_s$ (f_s is the sampling rate) [24], the sampling intervals in

each cell can be deduced accordingly. Figure 4 shows the sampling intervals obtained at 4.7 GS/s, where Fig. 4(a) presents the delay of 1024 sampling taps in DRS4, and Fig. 4(b) plots corresponding distribution of the delay. The sampling intervals alternate cell by cell, and the delay spreads into two distributions: one is centralized at 285.8 ps with a standard deviation of 23.6 ps, and the other at about 140.4 ps with a standard deviation of 23.5 ps. The average delay of the former distribution is about two times that of the latter, and the total variation of the 1024 sampling intervals is about 76 ps RMS. The results are consistent with those in Fig. 3.
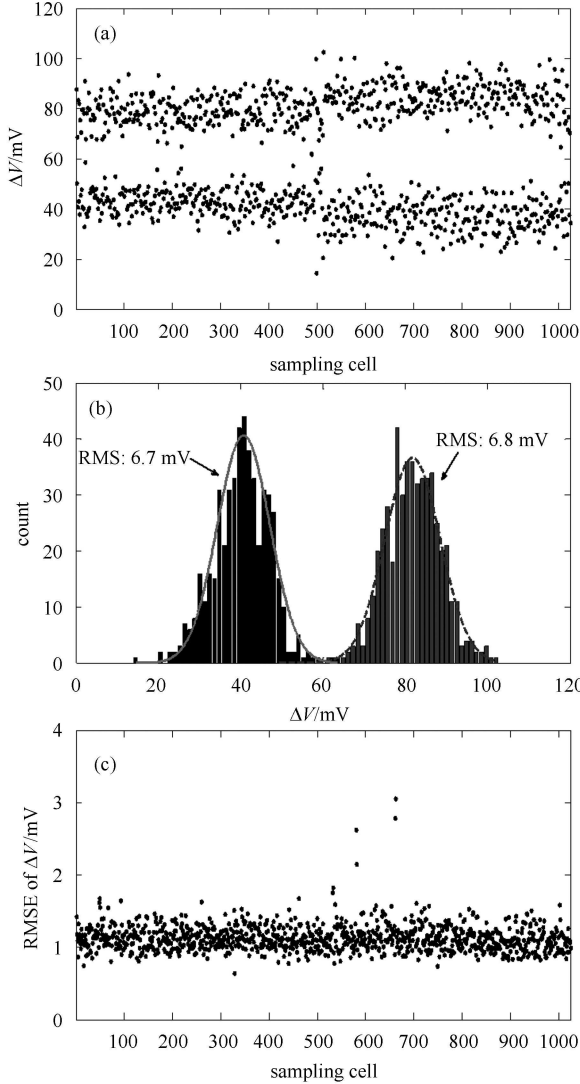

Fig. 3. (color online) Voltage differences with zero-crossing method, where (a) illustrates the zero-crossing voltage difference at each sampling cell (cell 1–1024), (b) shows the corresponding distribution, and (c) presents RMS of the variation of zero-crossing voltage differences in (a) for each cell.
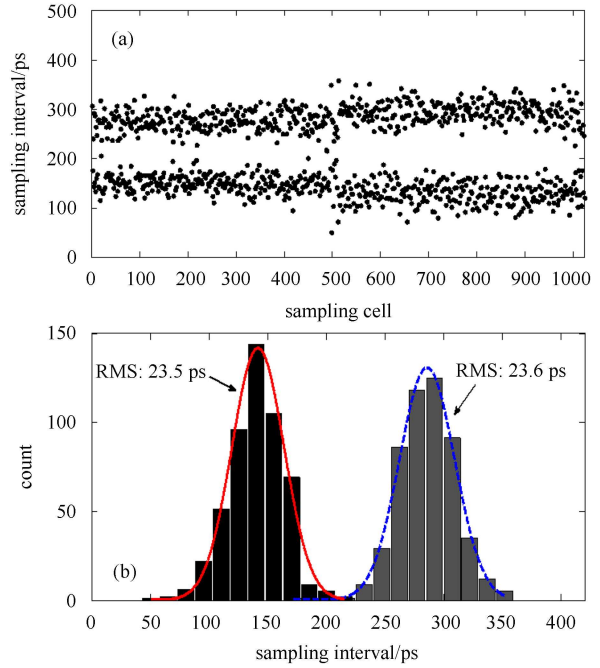

Fig. 4. (color online) Sampling intervals of DRS4 at 4.7 GS/s, in which (a) shows the sampling intervals at each sampling cell, and (b) presents the corresponding distribution.
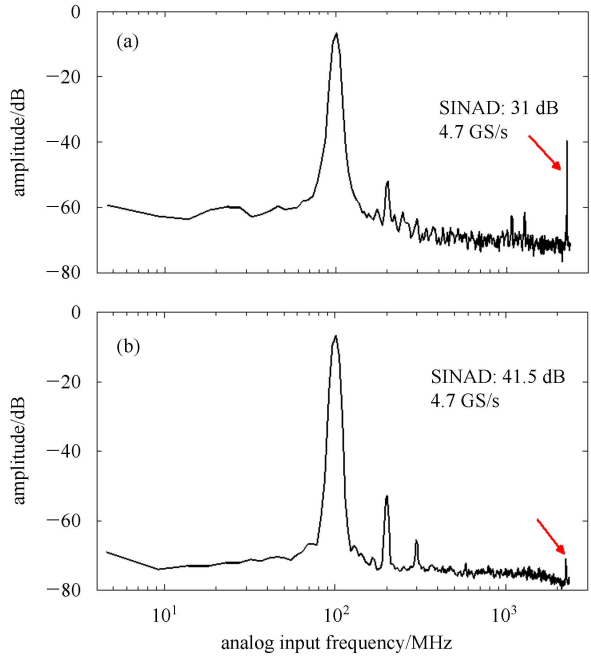

Fig. 5. (color online) Spectrum analysis of the sine samples, in which (a) shows the spectrum before calibration of uneven sampling intervals, whereas (b) presents that after calibration.

2.2   Verification of the sampling intervals

The sampling intervals derived above show very large variation and are spread into two distributions. Thus,

waveform digitization with the module is subject to non-uniform sampling. We perform spectrum analysis of the raw samples, expecting large distortions at $\pm f_{in} + f_s/2$ (f_{in} is the sine frequency) [28]. This is verified by the spectrum analysis in Fig. 5(a). There is a large distortion at about 2.247 GHz (marked with a red arrow), which is about $f_s/2 - f_{in} = 4.7$ GHz/2–100 MHz=2.25 GHz. We then interpolate the raw samples with uniform sampling intervals, and plot the corresponding spectrum in Fig. 5(b). We observe that the distortion gets smaller. Besides, the signal to noise and distortion ratio (SINAD) is also improved from 31 dB to 41.5 dB. The improvement of the spectrum performance reflects that the sampling intervals derived in Fig. 4 are a good representation of the tap delay in DRS4. Note there are second and third order distortions in Fig. 5. These distortions

Fig. 6. (color online) Distribution of the pulse delay derived from waveform sampling, where (a) shows the delay distribution before calibration of the non-uniform sampling intervals, (b) presents that after calibration, and (c) shows the time distribution with both low-pass noise suppression and uneven sampling interval compensation.

come from the sine signal generator and the band-pass filters used in our test. The spectra in Fig. 5 are performed by averaging about 200 individual FFTs of 100 MHz sine samples.

2.3 Timing performance with the sampling intervals

We apply the sampling intervals in Fig. 4 to the pulse delay test in Ref. [23]. In the test, one pulse is split into two with additional delay in one of them. The module samples the pulses, and we perform a 6-order polynomial fitting of the leading edges. The arrival time of a pulse is derived from the crossing time of a digital threshold (200 mV, 800 mV amplitude) on the leading edges. Fig. 6 shows the time delay, in which Fig. 6(a) presents the time distribution before uneven sampling intervals calibration, Fig. 6(b) shows that after calibration, and Fig. 6(c) shows the time distribution with both calibration of uneven sampling intervals and low-pass suppression as in [23]. The timing performance is improved from 16.8 ps RMS to 8.8 ps RMS after non-uniform sampling interval calibration. There is no significant improvement on timing performance after further processing the calibrated results with low-pass noise suppression (8.6 ps RMS). From this point of view, the low pass noise suppression filter in Ref. [23] is no longer essential after aligning the samples with the non-uniform sampling intervals derived here.

3 Waveform timing performance of the module in a cosmic ray telescope

We built a cosmic ray telescope with plastic scintillators and fast PMTs similar to that in Ref. [27], and put the module in this setup for readout. Different algorithms are employed for waveform timing analysis, and the timing performance of the module is compared with that of the oscilloscope in Ref. [27].

3.1 Setup of the experiment

The setup of the experiment is shown in Fig. 7. Two identical plastic scintillator bars (EJ200 [29]) 2360 mm long and 50 mm thick are placed one over the other. The four ends of the scintillators are coupled via four GDB60 PMTs [30] (PMT1-4, 900 ps rise time), and pulses from these are transmitted to the module for digitization. Cosmic rays strike EJ200 from a wide range of solid angles. However, we only choose the portion passing through the middle for a better characterization of the timing performance [27]. The selection is done with coincidences of pulses from two scintillator-PMT pairs placing in the middle of EJ200 (Scintillator: BC-420 [31]; PMT5, PMT6: XP2020 [32]). Anytime there is
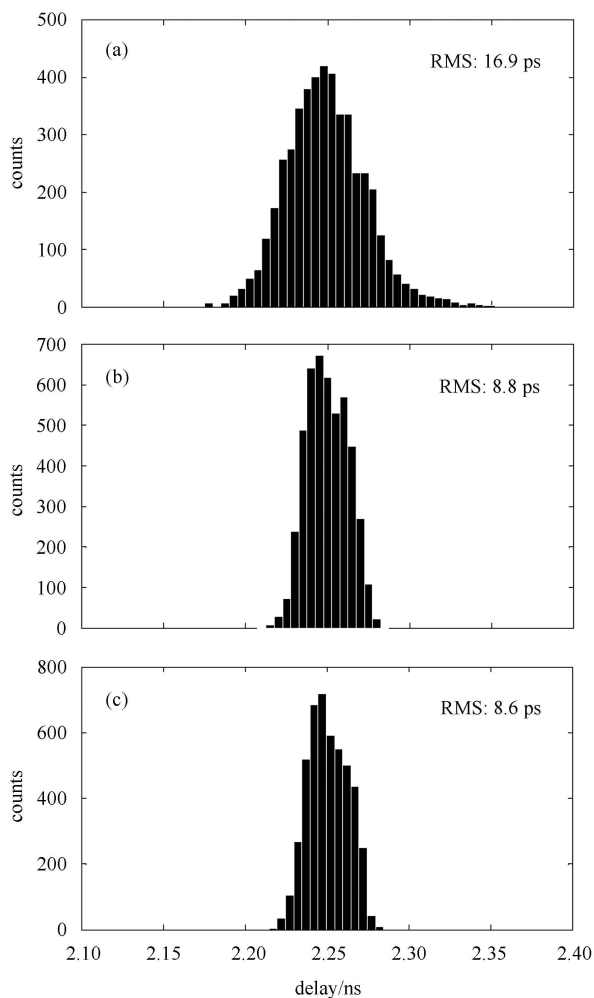
a coincidence, the module will be triggered to record the pulses from PMT 1–4. Typical waveforms are shown in Fig. 8. The area of each BC-420 scintillator is around 50 mm×50 mm, and is relatively small with respect to the area of EJ200. Therefore EJ200 can be considered to be struck vertically in the middle by the selected cosmic rays.
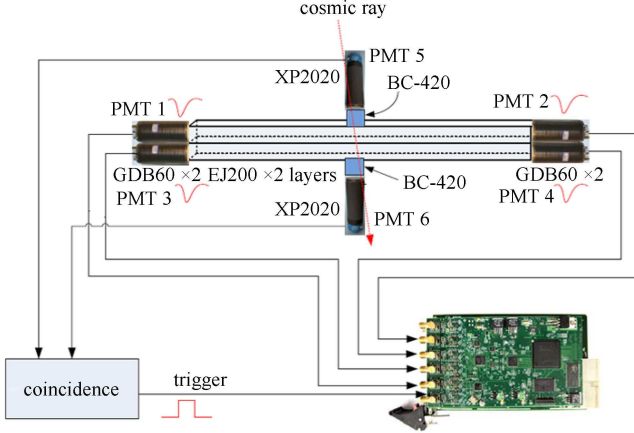

Fig. 7.   (color online) Experimental setup of the cosmic ray telescope.
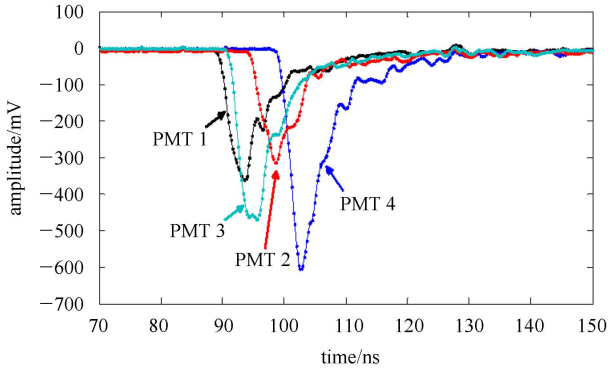

Fig. 8.   (color online) Typical waveforms from four ends of scintillators (EJ200).

We extract the arrival time of pulses from PMT 1–4, t_1, t_2, t_3, and t_4, from their waveforms, and estimate the timing performance from the standard deviation of the average time (t) defined as follows:

$$t=[(t_1+t_2)-(t_3+t_4)]/4. \tag{1}$$

The definition in (1) reduces the variation of hit positions of cosmic rays, and the uncertainty of the referencing time [27].

3.2   Waveform timing algorithms

There are several techniques for time extraction from sampled waveforms, such as leading edge discrimination with one or multiple thresholds, digital constant fraction zero-crossing, and pulse shape fitting. A good introduction and comparison of these is given in Refs. [4, 33, 34]. Among these algorithms, some require a constant shape of detector signals, such as the χ^2 approach and optimal filtering [34]. These are not suitable for our application, since we sample the waveform without any shaping circuits. Though it is possible to implement pulse shaping with digital signal processing, we are more interested in the information carried by the original waveforms. The algorithms we will use are: digital constant fraction discrimination (d-CFD), cross correlation, and amplitude-weighted sliding window.

d-CFD derives the arrival time from the crossing time at a constant fraction of the pulse amplitude. Cross correlation is a measure of the similarity of two pulses. With the setup in Fig. 7, we perform cross correlation of pulses from PMT 1 and PMT 3, PMT 2 and PMT 4, respectively. The time corresponding to the maximum point in the cross correlation waveform represents the time difference, i.e., t_1-t_3, and t_2-t_4. The average time t is then obtained from (1). In our evaluation, cross correlation of two vectors x and y is calculated from the inverse Fast Fourier Transform of the product: $X^*(\mathrm{e}^{\mathrm{j}w})\times Y(\mathrm{e}^{\mathrm{j}w})$. $X(\mathrm{e}^{\mathrm{j}w})$ and $Y(\mathrm{e}^{\mathrm{j}w})$, are the Fast Fourier Transform (FFT) of x and y, respectively. The operator $*$ on the top right of A (A^*) computes the complex conjugate of A.

The amplitude-weighted sliding window extracts the arrival time of pulses (t_d) from amplitude weighted time in a defined time range (time window: w_s). The arrival time is computed as (2):

$$t_d = \frac{\displaystyle\sum_{i=i_0}^{i_0+w_s-1} s_i \times t_d(i)}{\displaystyle\sum_{i=i_0}^{i_0+w_s-1} s_i}. \tag{2}$$

In (2), i is the sample index, starting from i_0 and covering a window size of w_s. s_i and $t_d(i)$ are the amplitude and time stamp of the i-th sample. A detailed introduction of this algorithm can be found in Ref. [11].

3.3   Waveform timing performance

In Table 1, we evaluate the waveform timing performance of the module in the cosmic ray telescope with the three algorithms mentioned in Section 3.2, and compare the results with that of the oscilloscope [27]. For consistency in comparison, the raw data of the oscilloscope in Ref. [27] are reprocessed in an identical way as that of the module, and the obtained timing performance is used for comparison.

In Table 1, the timing performance is for the two-ended readout of a scintillator bar, therefore the timing variation is $1/\sqrt{2}$ of that in (1). For the module, we list

waveform timing performance without and with uneven sampling intervals calibration (denoted as Raw and Calibrated respectively). For the oscilloscope, we also show the timing performance at 5 GS/s in addition to that at 10 GS/s. The oscilloscope works at 10 GS/s, and 5 GS/s is achieved by extracting one sample out of every two samples.

Table 1.   Comparison of waveform timing performance.

algorithms	timing performance (RMS: ps)			
	the module		oscilloscope in [27]	
	raw	calibrated	10 GS/s	5 GS/s
d-CFD	52	48.5	52.3	52.1
sliding window	53.8	52.8	48.7	51.1
cross correlation	57.2	55.8	61.0	59.3

For d-CFD, we apply a fourth-order polynomial fitting of samples within 0.05%–30% height in leading edges, and the arrival time is derived from the crossing time of 15% of the pulse height. For amplitude-weighted sliding window, we also choose samples within 0.05%–30% pulse height in leading edges for calculation. Cross correlation is performed by first interpolating the sampling step to be 20 ps for better precision. Interpolation is done via the spline function in Matlab [35].

We observe in Table 1 that the timing performance achieved with the module and the oscilloscope are both around 50 ps RMS. A typical time distribution is shown in Fig. 9. There is a slight improvement in the timing performance after non-uniform sampling interval calibration for the module. The timing performance for the oscilloscope at 10 GS/s and 5 GS/s are also comparable. The waveform timing precision of the module is proved to be about 10 ps RMS, and it is negligible with respect to the timing variation in Table 1 (∼50 ps RMS). Therefore, Table 1 reflects the potential waveform timing precision of the setup in Fig. 7.
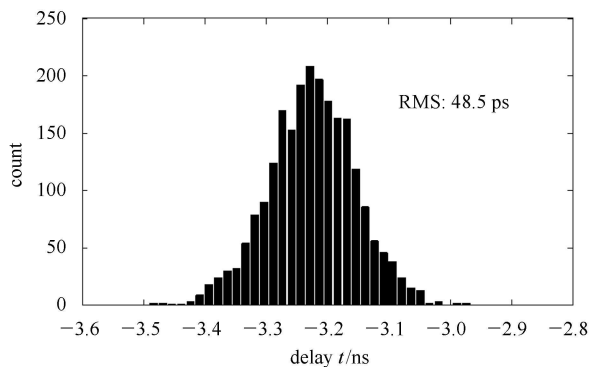

Fig. 9.   (color online) Typical time distribution of t.

4   Discussion

4.1   Sampling intervals variation of DRS4

The sampling intervals of DRS4 derived in Section 2.1

show much larger variation than those with a pre-signal processing of low-pass filtration in [23]. Good performances are achieved in both cases. However with verification of spectral analysis in Section 2.2, we consider the sampling intervals derived here to be a more accurate representation of the sampling tap delay in DRS4. This is consistent with a recent report about DRS4 from Dr. Stefan Ritt [36]. Moreover, with such sampling intervals, no noise suppression strategies are required for the module to achieve sub-10 ps RMS timing precision.

Compensation of non-uniform sampling intervals of DRS4 is essential for applications with 20 ps RMS timing precision or less. However for those with timing precision of 50 ps RMS or above, such compensation is not essential since no significant timing performance improvement will be obtained. This is reflected in Table 1 for the setup in Fig. 7.

4.2   Potential applications in TOF experiments

The timing resolution of current TOF systems has been of the order of 100 ps for several decades [1, 2, 37, 38], e.g., the timing resolution is 78 ps in the BESIII barrel TOF system [38]. In [27], it is proved that waveform timing is very promising to improve timing resolution in TOF systems. The authors used an oscilloscope in a similar setup as Fig. 7, and a timing resolution of ∼50 ps was achieved. In Section 3, we found comparable timing performance can be obtained with our module. We summarize the comparison in Table 2.

Table 2.   Comparison of the module and the oscilloscope.

parameter	the module	the osicilloscope [27]
sampling Rate	4.7 GS/s (max.)	10 GS/s
bandwidth	600 MHz	1 GHz
channels	6	4
dynamic Range	1 V/0.35 mV	10 V/25 mV
(V_{pp}/V_{rms})[a]	≈2860 [23]	≈400 [27]
power	∼17.5 mW/channel for DRS4 at 2 GS/s [24]	- - - - - - - - [b]
sampling depth	1 K /channel [24]	1 M/channel [26]

a V_{pp} is the input voltage range, e.g., for the module in Fig. 7, V_{pp}=1 V. V_{rms} is the voltage noise for DC input.

b No literature found on the power of ADC used in the oscilloscope.

From comparison in Table 2, we find the module with DRS4 features such advantages as high channel density (6 of the 8 channels in the DRS4 are used in the current module), low power consumption, and high dynamic range for input with respect to the oscilloscope. From these points of view, modules with DRS4 can be a good candidate for future TOF upgrade with waveform sampling. There are also drawbacks for DRS4 in limited sampling depth and larger dead time for readout (of the order of one microsecond, depending on the working mode of

DRS4) [24]. However, these will no longer be a problem for DRS5, the fifth version of DRS [39]. Besides, we can also integrate the timing algorithms as amplitude-weighted sliding window and cross correlation on readout electronics. In this way, we are able to alleviate the requirement on data transmission bandwidth by sending the extracted time, instead of the whole waveform.

5   Conclusion

We clarified non-uniform sampling intervals of a fast pulse sampling module with DRS4. The sampling intervals were derived by zero-crossing of sine waves, and verified by spectrum analysis. We then evaluated the performance of the module in a cosmic ray setup with plastic scintillators and fast PMTs. Different algorithms were used for waveform timing analysis, and the timing performance found to be comparable to a 10 GS/s oscilloscope in a similar setup.

References

1 Kichimi H, Yoshimura Y, Browder T et al. Nucl. Instrum. Methods in Physics Research A, 2000, **453**: 315–320
2 Paus C, Grozis C, Kephart R et al. Nucl. Instrum. Methods in Physics Research A, 2001, **461**: 579–581
3 BESIII Collaboration. Nucl. Instrum. Methods in Physics Research A, 2009, **598**: 7–11
4 Genat J, Varner G, TANG F et al. Nucl. Instrum. Methods in Physics Research A, 2009, **607**: 387–393
5 Breton D, Delagnes E, Maalmi J et al. Nucl. Instrum. Methods in Physics Rearch A, 2011, **629**: 123–132
6 Dhawan S, Hughes V, Kawall D et al. Nucl. Instrum. Methods in Physics Rearch A, 2000, **450**: 391–398
7 Kornilov N, Khriatchkov V, Dunaev M et al. Nucl. Instrum. Methods in Physics Rearch A, 2003, **497**: 467–478
8 Bartko H, Goebel F, Mirzoyan R et al. Nucl. Instrum. Methods in Physics Rearch A, 2005, **548**: 464–486
9 Becvar F, Cizek J, Prochazka I. Nucl. Instrum. Methods in Physics Rearch A, 2005, **539**: 372–385
10 Mihailescu L, Borcea C, Plompen A. Nucl. Instrum. Methods in Physics Rearch A, 2007, **578**: 298–305
11 Albert J, Aliu E, Anderhub H et al. Nucl. Instrum. Methods in Physics Rearch A, 2008, **594**: 407–419
12 Mihailescu L, Borella A, Massimi C et al. Nucl. Instrum. Methods in Physics Rearch A, 2009, **600**: 453–459
13 Ritt S. Nucl. Instrum. Methods in Physics Research A, 2002, **494**: 520–525
14 Pegna R, Cecchi R, Paoletti R et al. Nucl. Instrum. Methods in Physics Research A, 2006, **567**: 218–221
15 Pegna R, Barcelo M, Bitossi M et al. Nucl. Instrum. Methods in Physics Research A, 2007, **572**: 382–384
16 Ritt S, Dinapoli R, Hartmann U. Nucl. Instrum. Methods in Physics Research A, 2010, **623**: 486–488
17 Lachartre D, Feinstein F. Nucl. Instrum. Methods in Physics Research A, 2000, **442**: 99–104
18 Delagnes E, Degerli Y, Goret P et al. Nucl. Instrum. Methods A, 2006, **567**: 21–26
19 Ruckman L, Nishimura K, Varner G et al. Nucl. Instrum. Methods in Physics Research A, 2010, **623**: 303–305
20 Varner G, Ruckman L, Nam J et al. Nucl. Instrum. Methods in Physics Research A, 2007, **583**: 447–460
21 Varner G, Ruckman L, Wong A. Nucl. Instrum. Methods in Physics Research A, 2008, **591**: 534–545
22 Ritt S. In Nucl. Design and Performance of the 6 GHz Waveform Digitizing Chip DRS4. In: Sci. Symp. Conf. Rec, Oct. 2008. 1512–1515
23 WANG J, ZHAO L, FENG C et al. IEEE Trans. Nucl. Sci, 2012, **59**(5): 2435–2443
24 DRS4 User Guide. Rev.0.9, Paul Scherrer Institute, 2008
25 WANG J, ZHAO L, FENG C et al., Nucl. Sci. & Technology, 2012, **23**(2): 109–113
26 Lecroy WavePro 7100 series, www.lecroy.com
27 LI S, HENG Y, ZHAO T et al. Chinese Physics C, 2013, **37**(1): 016003-(1-6)
28 Kurosawa N, Kobayashi H, Maruyama K et al. IEEE Trans. Circuits Syst. I, Fundam. Theory and Appl., 2001, **48**(3)
29 EJ200 Plastic Scintillators Data Sheet, ELJEN Technology Corporation. www.eljentechnology.com
30 GDB 60 PMT Data Sheet. Beijing energy Science & Technology Co., Ltd. www.beijing-energy.com
31 BC-420 Premium Plastic Scintillators Data Sheet. Saint-Gobain Crystals. www.detectors.saint-gobain.com
32 XP2020 PMT Data Sheet. Photonis USA Pennsylvania, Inc. July, 2007
33 Nelson M, Rooney B, Dinwiddie D et al. Nucl. Instrum. Methods in Physics Research A, 2003, **505**: 324–327
34 Cleland W E et al. Nucl. Instrum. Methods in Physics Research A, 1994, **338**: 467–497
35 The MathWorks. Inc. Version 7.14.0.739
36 Ritt S. HAP Topic 4 Workshop, Germany, January, 2013. www.psi.ch/drs/documentation
37 Klempt W. Nucl. Instrum. Methods in Physics Research A, 1999, **433**: 542–553
38 HENG Y. In Nucl. Sci. Symp. Conf. Rec., Oct. 2007. 53–56
39 Ritt S. Plans for the DRS5 Switched Capacitor Array. In: Picosecond Workshop 2011. http://drs.web.psi.ch/docs